Gustafsson, Tom; Hakula, Harri; Leinonen, Matti

Stochastic Galerkin approximation of the Reynolds equation with irregular film thickness

Published in:
Computers and Mathematics with Applications

DOI:
10.1016/j.camwa.2017.06.012

Published: 01/10/2017

Document Version
Peer-reviewed accepted author manuscript, also known as Final accepted manuscript or Post-print

Please cite the original version:
Gustafsson, T., Hakula, H., & Leinonen, M. (2017). Stochastic Galerkin approximation of the Reynolds equation with irregular film thickness. *Computers and Mathematics with Applications*, *74*(7), 1590-1606. https://doi.org/10.1016/j.camwa.2017.06.012

Stochastic Galerkin approximation of the Reynolds equation with irregular film thickness

Tom Gustafsson[1], Harri Hakula[2], Matti Leinonen

Aalto University
Department of Mathematics and System Analysis
P.O. Box 11100
FI–00076 Aalto, Finland

Abstract

We consider the approximation of the Reynolds equation with an uncertain film thickness. The resulting stochastic partial differential equation is solved numerically by the stochastic Galerkin finite element method with high-order discretizations both in spatial and stochastic domains. We compute the pressure field of a journal bearing in various numerical examples that demostrate the effectiveness and versability of the approach. The results suggest that the stochastic Galerkin method is capable of supporting design when manufacturing imperfections are the main sources of uncertainty.

Keywords: Reynolds equation, sGFEM, stochastic surfaces

1. Introduction

Solving partial differential equations robustly in domains with random boundaries is necessary to predict the consequences of, e.g., manufacturing faults and wear defects. A universal approach is to transform the random

Email addresses: `Tom.Gustafsson@aalto.fi` (Tom Gustafsson), `Harri.Hakula@aalto.fi` (Harri Hakula), `Matti.Leinonen@aalto.fi` (Matti Leinonen)

[1]The work of T. Gustafsson has been funded by the Finnish Cultural Foundation and Tekes (the Finnish Funding Agency for Innovation).

[2]The work of H. Hakula has received funding from the European Research Council under the European Unions Seventh Framework Programme (FP7/2007–2013) ERC grant agreement no 339380.

domain into a deterministic reference domain through a mapping that depends on a set of random variables [1]. The approach will in general modify the governing equation, possibly making it more complicated.

Although this seems to be an unavoidable consequence of introducing randomness in the domain of a boundary value problem, there exists a fairly large class of models where an alternative approach may suffice from an engineering viewpoint, namely the so-called dimension reduced models. It is typical for these models to incorporate the length scale in one or more dimensions—for example, the thickness of a plate or the width and height of a beam—as material parameters. This leads to an intriguing possibility of applying stochastic numerical methods that are suitable for the approximation of BVPs with random material fields to the solution of these dimension reduced models, essentially with random geometries. The focus of this work is on the stochastic Galerkin finite element method (sGFEM), cf. Bieri–Schwab [2].

A fairly typical property of the dimension reduced models is that the PDE depends on the reduced length parameter in a non-affine or polynomial manner. This is sometimes the case, e.g., in the theory of plates and shells [3], classical beam theories [4], fluid film lubrication [5] and duct acoustics [6]. As the stochastic input is most conveniently given in the form of a Karhunen–Loéve (KL) expansion, the resulting PDE with a random material parameter field depends on the random variables of the expansion also in a non-affine manner. In the context of sGFEM, this introduces a need to efficiently construct the related stochastic moment matrices [7].

In this study we discuss the approximation of the Reynolds equation with a stochastic film thickness. Reynolds equation describes the flow of fluids in problems where a thin film of lubricant oil is situated between two almost parallel surfaces [8]. The governing equation is a second-order elliptic PDE with the diffusion coefficient depending on the third power of the thickness of the film. For a physical example problem we have chosen the case of a journal bearing (e.g., Szeri [5] or Hamrock et al. [9]) where the film thickness is assumed to contain transverse variations due to nonidealities in the manufacturing process or due to fatigue wear. The structure of a journal bearing implies that the film thickness and, therefore, the pressure field are periodic. Thus, we define the variations in the film thickness through a cleverly constructed periodic random field. In the stochastic Reynolds equation the random film thickness is represented using the Karhunen–Loève expansion. Thus, there are many options for model reduction through truncation of the series and its powers.

The effect of incorporating surface roughness directly into the solution of the Reynolds equation has been studied using analytical methods in Tzeng–Saibel [10], Christensen [11] and, thereafter, by various other authors [12, 13, 14, 15]. An alternative modeling approach based on the homogenization of the surface roughness has recently gained interest [16, 17, 18]. Nonetheless, our work is based on the direct approximation of a stochastic Reynolds equation with a belief that this type of approach has the potential to combine larger scale variations due to, e.g., manufacturing flaws and smaller scale variations due to wear into a single model.

This paper features a thoroughly verified framework for performing stochastic Galerkin computations that combine high-order approximation both in spatial and stochastic dimensions. For a chosen reduced variant of the model, we obtain accurate predictions of the statistics of the hydrodynamic pressure field in a journal bearing under the assumption of an uncertain film thickness. The approach can be ultimately seen as a more complete and robust alternative to the traditional sensitivity analysis of journal bearings where the uncertainty is taken into account through maximum tolerances in the constant film thickness.

Some numerical work on the approximation of a stochastic lubrication model exists in hydrodynamic context. The approach of Turaga et al. [19, 20, 21] is to solve an approximate differential equation with the expected value of the pressure field as an unknown. The variance is then estimated using a first-order second-moment method. However, we are not aware of any studies employing the recent advances in sGFEM or the related pseudo-spectral methods in hydrodynamic problems. Recent studies that consider the effects of uncertain geometry in other contexts include, e.g., Xiu–Shen [22] for acoustic scattering from rough surfaces, Bierig–Chernov [23] for the random obstacle problem and Hyvönen–Mustonen [24] for the thermal tomography with uncertain boundary shape.

The rest of this paper is organized as follows: The necessary computational framework is outlined in Section 2; In Section 3 the stochastic Reynolds equation is introduced; An extensive set of numerical experiments are detailed in Section 4; The conclusions are discussed in Section 5. In the Appendix, the construction of periodic covariance is discussed, and the conjugate gradient method is outlined.

2. Preliminaries

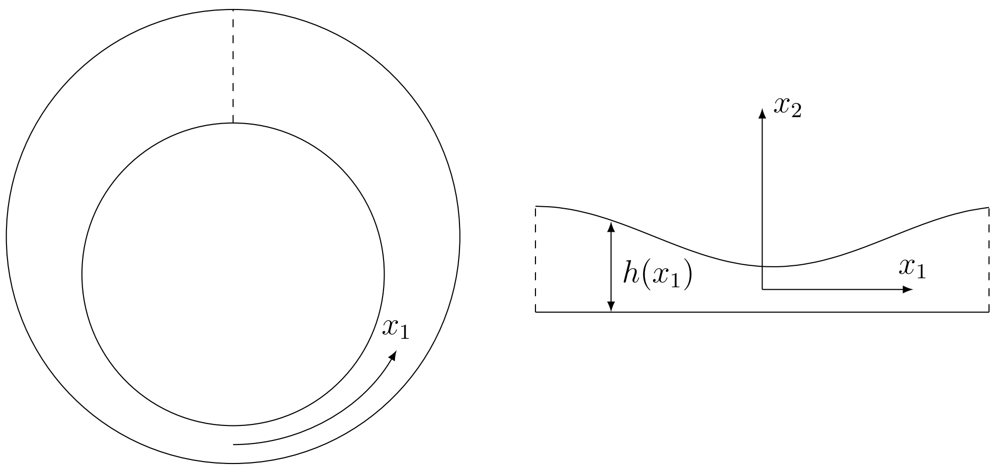

Figure 1: The geometry of the journal bearing and unraveling of the domain. Here the channel height $h(x_1) = 1 + \epsilon \cos(x_1 + \pi)$, $x_1 \in [-\pi, \pi]$, where $0 \leq \epsilon < 1$ is the eccentricity of the bearing.

This section introduces the building blocks of the stochastic lubrication model that will be presented in Section 3. We begin by deriving the classical lubrication approximation of the Navier–Stokes equations, often referred to as the Reynolds equation. Next we briefly introduce the necessary definitions related to non-affine random fields. We finish the section by discussing the weak formulation of a stochastic diffusion problem and its discretization through the Galerkin method.

2.1. Reynolds Equation

Consider the equations governing an isothermal flow of an incompressible viscous fluid,

$$\rho \left(\frac{\partial \boldsymbol{v}}{\partial t} + (\nabla \boldsymbol{v})\boldsymbol{v} \right) = -\nabla p + 2\mu \operatorname{div} \boldsymbol{D}(\boldsymbol{v}) + \rho \boldsymbol{b}, \tag{1}$$

$$\operatorname{div} \boldsymbol{v} = 0, \tag{2}$$

where $\boldsymbol{v}$ is the unknown velocity field, $\rho > 0$ is the constant density, $\mu > 0$ is the constant viscosity and $\boldsymbol{b}$ corresponds to the body force. Moreover, $\boldsymbol{D}(\boldsymbol{v}) = \frac{1}{2}(\nabla \boldsymbol{v} + \nabla \boldsymbol{v}^T)$ denotes the symmetric part of the velocity gradient and p is a scalar field associated with the incompressibility constraint (2)—often referred to as the mechanical pressure.

We consider stationary flows while assuming that the inertial effects and contribution of the body force can be neglected. This reduces the governing equations to the following Stokes system:

$$2\mu \operatorname{div} \boldsymbol{D}(\boldsymbol{v}) - \nabla p = 0, \tag{3}$$

$$\operatorname{div} \boldsymbol{v} = 0. \tag{4}$$

Next we restrict our attention to two-dimensional plane flows, i.e.

$$\boldsymbol{v} = (u(x_1, x_2), v(x_1, x_2)), \quad p = p(x_1, x_2). \tag{5}$$

The geometry is fixed to be that of a journal bearing, see Figure 1, where the fluid is situated in a thin cavity between the inner and outer surfaces. We may consider the relative importance of the different terms in (3) and (4) by arguing that in this setting the domain length in x_2-dimension is noticeably smaller than the domain length in x_1-dimension, see for example Szeri [5]. This will reduce the governing equations (3) and (4) to the following set of partial differential equations:

$$\mu \frac{\partial^2 u}{\partial x_2^2} = \frac{\partial p}{\partial x_1}, \tag{6}$$

$$\frac{\partial p}{\partial x_2} = 0, \tag{7}$$

$$\frac{\partial u}{\partial x_1} + \frac{\partial v}{\partial x_2} = 0. \tag{8}$$

Note that the equation (7) implies $p = p(x_1)$. Let the height of the flow channel be denoted by $h = h(x_1)$ and let U be the x_1-velocity of the outer surface. Integrating the equation (6) twice with respect to x_2 and applying the boundary conditions

$$u(x_1, h(x_1)) = 0, \quad u(x_1, 0) = U, \tag{9}$$

gives

$$u(x_1, x_2) = \frac{1}{2\mu} \frac{\partial p}{\partial x_1}(x_1)(x_2^2 - x_2 h(x_1)) + \left(1 - \frac{x_2}{h(x_1)}\right) U. \tag{10}$$

Next we integrate (8) with respect to x_2 to get

$$v(x_1, h(x_1)) - v(x_1, 0) = -\int_0^{h(x_1)} \frac{\partial u}{\partial x_1} \,\mathrm{d}x_2 \tag{11}$$

and, after substituting the equation (10) for u, we arrive at the Reynolds equation

$$\frac{\partial}{\partial x_1}\left(\frac{h^3}{\mu}\frac{\partial p}{\partial x_1}\right) = 6U\frac{\partial h}{\partial x_1} + 12(v(x_1, h(x_1)) - v(x_1, 0)). \tag{12}$$

The second term on the right hand side of (12) represents the velocity of approach of the bearing surfaces. In a quasi-static framework this would normally be zero owing to the fact that the bearing surfaces are in most cases assumed to be flat. We instead argue that the velocity of approach is proportional to the change in h, that is

$$12(v(x_1, h(x_1)) - v(x_1, 0)) \propto \frac{\partial h}{\partial x_1}. \tag{13}$$

This would be exactly the case when one of the surfaces was flat and the other necessarily was not. The resulting equation, with normalized material parameters and notation $x = x_1$, reads

$$\frac{\partial}{\partial x}\left(h^3\frac{\partial p}{\partial x}\right) = \frac{\partial h}{\partial x}. \tag{14}$$

The irregularity of the channel height will be introduced through a perturbation of h by a suitable random field.

2.2. Stochastic Input

The stochastic input is usually assumed to be given in the following *affine* form, often obtained using the Karhunen–Loève expansion; see, e.g., Adler–Taylor [25].

Definition 1 (Affine diffusion coefficient)**.** The affine diffusion coefficient is defined as

$$a(\omega, x) = a_0(x) + \sum_{m\geq 1} a_m(x)Y_m(\omega), \tag{15}$$

where $\{a_m\}_{m\geq 0}$ are some suitable spatial functions and $\{Y_m\}_{m\geq 1}$ is a family of random variables.

In our case, the parametric PDE (14) depends on the parameter h in a *non-affine* or *polynomial* manner. In fact, many relevant parametric PDEs are nonlinear and depend on the parameters in a similar way [26].

Definition 2 (Support of a multi-index)**.** The support of a multi-index $\eta \in \mathbb{N}_0^\infty$ is defined as $\operatorname{supp}\eta = \{m \in \mathbb{N} : \eta_m \neq 0\}$.

Definition 3 (Finitely supported multi-indices)**.** The set of finitely supported multi-indices $(\mathbb{N}_0^\infty)_c$ is defined by

$$(\mathbb{N}_0^\infty)_c = \{\eta \in \mathbb{N}_0^\infty : |\operatorname{supp}\eta| < \infty\} \subset \mathbb{N}_0^\infty,$$

where we use $|\operatorname{supp}\eta|$ to denote the number of elements in $\operatorname{supp}\eta$.

Definition 4 (Non-affine diffusion coefficient)**.** The non-affine diffusion coefficient is given by

$$a(\omega, x) = a_0(x) + \sum_{\mu\in\Xi} a_\mu(x) Y^\mu(\omega), \tag{16}$$

where $\Xi \subset (\mathbb{N}_0^\infty)_c$, a_0 and $\{a_\mu\}_{\mu\in\Xi}$ are some suitable spatial functions, and

$$Y^\mu(\omega) := \prod_{m=1}^{\infty} Y_m^{\mu_m}(\omega) = \prod_{m\in\operatorname{supp}\mu} Y_m^{\mu_m}(\omega).$$

As expected, the non-affine case includes the affine case; by selecting $\Xi = \{\mu \in (\mathbb{N}_0^\infty)_c \,|\, \mu = \mathrm{e}_n \text{ for some } n \in \mathbb{N}\}$, where e_n denotes the nth Euclidean basis vector of $\mathbb{R}^\infty$, the non-affine case reduces to the affine case.

2.3. Model Problem

Let $D \subset \mathbb{R}^d$, $d \in \mathbb{N}$, be a bounded domain with a smooth enough boundary. Consider the following model elliptic diffusion problem: Let (Ω, Σ, P) be a probability space. Find a random field $u \in L_P^2(\Omega, H_0^1(D))$ such that

$$\begin{cases} -\nabla\cdot(a(\omega,x)\nabla u(\omega,x)) = f(x), & \text{in } D, \\ u(\omega,x) = 0, & \text{on } \partial D, \end{cases} \tag{17}$$

holds P-almost surely for a load $f \in L^2(D)$ and a given strictly positive diffusion coefficient $a \in L^\infty(\Omega\times D)$ with lower and upper bounds $a_{\min}, a_{\max}$ such that

$$P\left(\omega\in\Omega \;:\; 0 < a_{\min} \le \operatorname*{ess\,inf}_{x\in D} a(\omega,x) \le \operatorname*{ess\,sup}_{x\in D} a(\omega,x) \le a_{\max}\right) = 1. \tag{18}$$

Here $L^2_P(\Omega, H^1_0(D))$ is a Bochner space with the norm

$$\|w\|^2_{L^2_P(\Omega,H^1_0(D))} = \int_\Omega \|w(\omega)\|^2_{H^1_0(D)} \, \mathrm{d}P(\omega).$$

See, e.g., Schwab–Gittelson [27] and the references therein for more information.

A standard approach is to transform the model problem (17) into a parametric deterministic form by first assuming the family $\{Y_m\}_{m\geq 1} : \Omega \to \mathbb{R}$ to be *mutually independent* with ranges Γ_m and associating each Y_m with a complete probability space $(\Omega_m, \Sigma_m, P_m)$, where the probability measure P_m admits a probability density function $\rho_m : \Gamma_m \to [0, \infty)$ such that

$$\mathrm{d}P_m(\omega) = \rho_m(y_m) \, \mathrm{d}y_m, \quad y_m \in \Gamma_m,$$

and the σ-algebra Σ_m is assumed to be a subset of the Borel sets of Γ_m. Finally, it is assumed that the stochastic input is *finite*, i.e., in the affine case we assume that there exists $\mathcal{M} < \infty$ such that $Y_m = 0$, when $m > \mathcal{M}$, which essentially truncates the series in (15) after $\mathcal{M}$ terms, and in the non-affine case (16) we assume that the set Ξ has a finite number of elements and $\mathcal{M}$ as in the affine case exists. Notice, that instead of assuming that the parameters Y_m are mutually in- dependent, independence can be ensured for instance through a suitable isoprobabilistic transformation.

After these assumptions the parametric deterministic weak formulation of (17) is to find $u \in L^2_\rho(\Gamma, H^1_0(D))$ that satisfies

$$\int_\Gamma \int_D a(y,x) \nabla u(y,x) \cdot \nabla v(y,x) \rho(y) \, \mathrm{d}x \, \mathrm{d}y = \int_\Gamma \int_D f(x) v(y,x) \rho(y) \, \mathrm{d}x \, \mathrm{d}y, \tag{19}$$

for all $v \in L^2_\rho(\Gamma, H^1_0(D))$, where $y := (y_1, y_2, \cdots) \in \Gamma := \Gamma_1 \times \Gamma_2 \times \cdots$ and $\rho(y) \, \mathrm{d}y := \prod_{m\geq 1} \rho_m(y_m) \, \mathrm{d}y_m$. There exists a unique solution to (19) which is a consequence of the Lax–Milgram lemma.

By discretization, the weak formulation (19) reduces to the following linear system of equations in the affine case (15):

$$\left(G_0 \otimes A_0 + \sum_{m=1}^{\mathcal{M}} G_m \otimes A_m \right) \boldsymbol{u} = g_0 \otimes f_0, \tag{20}$$

where $\{A_m\}_{m=0}^{\mathcal{M}}$ are standard FEM matrices, f_0 is a standard load vector, $\{G_m\}_{m=0}^{\mathcal{M}}$ are stochastic moment matrices, and g_0 is a stochastic load vector; see Bieri–Schwab [2] for details.

For the stochastic load vector and moment matrices, we recall that each multi-index $\eta \in (\mathbb{N}_0^\infty)_c$ determines a multivariate polynomial $\Phi_\eta(y)$.

Definition 5 (Multivariate polynomial)**.** Let $\eta \in (\mathbb{N}_0^\infty)_c$. The multivariate polynomial $\Phi_\eta(y)$, also called chaos polynomial, is defined as

$$\Phi_\eta(y) = \prod_{m=1}^{\infty} \phi_{\eta_m}(y_m) = \prod_{m \in \operatorname{supp} \eta} \phi_{\eta_m}(y_m), \tag{21}$$

where $\{\phi_m\}_{m \geq 0}$ is a suitably orthonormalized (univariate) polynomial sequence with $\phi_0 = 1$.

Let $\Lambda \subset (\mathbb{N}_0^\infty)_c$ be finite and consist of suitably chosen finitely supported multi-indices; see Schwab–Gittelson [27] and the references therein for more information. In order to enumerate the set Λ we use the function $\gamma_\Lambda : \{1, \cdots, |\Lambda|\} \to \Lambda$ which is defined so that it is bijective. In the affine case, the stochastic load vector g_0 is given by

$$\left[g_0\right]_i := \int_\Gamma \Phi_{\gamma_\Lambda(i)}(y)\rho(y)\,\mathrm{d}y \tag{22}$$

and the elements of the stochastic moment matrices are

$$\left[G_0\right]_{i,j} := \int_\Gamma \Phi_{\gamma_\Lambda(i)}(y)\Phi_{\gamma_\Lambda(j)}(y)\rho(y)\,\mathrm{d}y \qquad \text{and} \tag{23}$$

$$\left[G_m\right]_{i,j} := \int_\Gamma y_m \Phi_{\gamma_\Lambda(i)}(y)\Phi_{\gamma_\Lambda(j)}(y)\rho(y)\,\mathrm{d}y, \quad m \geq 1, \tag{24}$$

where $i, j \in \{1, \cdots, |\Lambda|\}$. In an ideal case, the index set Λ is chosen so that the linear combination

$$\sum_{\mu \in \Lambda} u_\mu(x)\Phi_\mu(y),$$

where $u_\mu := \int_\Gamma u(y, \cdot)\Phi_\mu(y)\rho(y)\,\mathrm{d}y \in H_0^1(D)$, gives a good approximation to the solution of (19). It is known that the stochastic moment matrices $\{G_m\}_{m=1}^{\mathcal{M}}$ exhibit a nontrivial sparsity pattern [2].

In the non-affine case (16), the resulting linear system is (cf. (20))

$$\left(G_0 \otimes A_0 + \sum_{\mu \in \Xi} G^\mu \otimes A_\mu \right) \boldsymbol{u} = g_0 \otimes f_0, \tag{25}$$

where A_0 and $\{A_\mu\}_{\mu\in\Xi}$ are standard FEM matrices and the stochastic moment matrices $\{G^\mu\}_{\mu\in\Xi}$ are given by

$$\left[G^\mu\right]_{i,j} := \int_\Gamma \left(\prod_{m=1}^{\infty} y_m^{\mu_m}\right) \Phi_{\gamma_\Lambda(i)}(y)\Phi_{\gamma_\Lambda(j)}(y)\rho(y)\,\mathrm{d}y \tag{26}$$

with i and j as above. Using this notation the matrix G_m, $m\in\mathbb{N}$, is given by G^{e_m} and G_0 is given with $\mu=(0,0,\cdots)$. As above, these moment matrices employ a nontrivial sparsity pattern.

In the case of an uncertain load, i.e. $f=f(\omega,x)$ in (17), the right hand side of the systems (20) and (25) is

$$g_0\otimes f_0+\sum_{\mu\in\Xi} g_\mu\otimes f_\mu, \tag{27}$$

where the vectors g_μ are natural basis vectors (assuming normalization), and f_μ are the corresponding FEM load vectors.

2.4. Convergence of Jacobi coefficients

Let $P(\alpha,\beta)_\nu$, $\nu\in\mathbb{N}_0$, denote the Jacobi polynomials that are scaled to be orthonormal with respect to the weighted inner product $(\cdot,\cdot\ w(x))_{L^2([-1,1])}$, where the weight $w(x)$ is the probability density function of the beta distribution

$$\rho(x;\alpha,\beta)=\frac{(1+x)^\alpha(1-x)^\beta}{2^{\alpha+\beta+1}\,\mathrm{B}(\alpha+1,\beta+1)},$$

where $\alpha>-1$, $\beta>-1$, and the beta function B is defined in terms of gamma functions as $\mathrm{B}(a,b)=\frac{\Gamma(a)\Gamma(b)}{\Gamma(a+b)}$. The multivariate Jacobi polynomials

$$P(\alpha,\beta)_\lambda := P(\alpha,\beta)_{\lambda_1}P(\alpha,\beta)_{\lambda_2}\cdots,\quad \lambda\in(\mathbb{N}_0^\infty)_c, \tag{28}$$

form a complete orthonormal basis for the Lebesgue space $L^2_\rho(\Gamma)$. The discretization in the parameter domain Γ will be achieved by expanding $u\in L^2_\rho(\Gamma;H^1_0(D))$ into this basis,

$$u=\sum_{\lambda\in(\mathbb{N}_0^\infty)_c} P(\alpha,\beta)_\lambda u_\lambda \tag{29}$$

with *Jacobi coefficients* $u_\lambda\in H^1_0(D)$. Parseval's theorem states that

$$u\in L^2_\rho(\Gamma;H^1_0(D)) \iff z:=\big(\,\|u_\lambda\|_{H^1_0(D)}\,\big)_{\lambda\in(\mathbb{N}_0^\infty)_c}\in\ell^2\big((\mathbb{N}_0^\infty)_c\big). \tag{30}$$

For any collection $\Lambda \subset (\mathbb{N}_0^\infty)_c$ we define the truncation operator T_Λ on $L^2_\rho(\Gamma; H^1_0(D))$ by truncating the Jacobi expansion (29) as

$$T_\Lambda : u \mapsto T_\Lambda u := \sum_{\lambda \in \Lambda} P(\alpha, \beta)_\lambda u_\lambda, \tag{31}$$

which in the case of trivial Λ evaluates to zero.

In the following, the set Λ is always an isotropic total degree index set.

Definition 6 (Isotropic total degree index set)**.** Let $N \in \mathbb{N}$ and $K \in \mathbb{N}_0$. The isotropic total degree index set is given as

$$\Lambda(N, K) = \left\{ \eta \in (\mathbb{N}_0^\infty)_c : \sum_{n=1}^{N} \eta_n \leq K;\ \eta_n = 0,\ n > N \right\}. \tag{32}$$

By quantifying the domain of analytic dependence of the exact solution $u \in L^2_\rho(\Gamma; H^1_0(D))$ of the model problem on the vector of parameters $y \in \Gamma$, an estimate on the convergence rate of the expansion (29) was obtained by Cohen, DeVore and Schwab in [28, Theorem 4.1] for Legendre polynomials, that is, the choice of $P(0, 0)$.

Theorem 1. *Assume that the diffusion coefficient a satisfies the positivity condition* (18) *and that the sequence $\left(\|a_m\|_{L^\infty(D)} \right)_{m \geq 1}$ is in $\ell^\tau(\mathbb{N})$ for some $\tau \in (0, 1)$. Let u be the exact solution to the variational formulation* (19)*, and let z denote the sequence of $H^1_0(D)$ norms of its Legendre coefficients, see* (30)*. Then $z \in \ell^\tau\big((\mathbb{N}_0^\infty)_c\big)$.*

Moreover, if $\Lambda \subset (\mathbb{N}_0^\infty)_c$ are the multi-indices of $|\Lambda|$ largest z_λ then

$$\|u - T_\Lambda u\|_{L^2_\rho(\Gamma; H^1_0(D))} \leq |\Lambda|^{-r} \|z\|_{\ell^\tau((\mathbb{N}_0^\infty)_c)}, \quad r = \frac{1}{\tau} - \frac{1}{2}, \tag{33}$$

where T_Λ is the truncation operator corresponding to (31)*.*

Extension of the theorem to cover all Jacobi polynomials remains an open problem. However, there is a growing body of evidence supporting the following conjecture.

Conjecture 2 (Convergence of Jacobi Coefficients)**.** *The rate predicted by Theorem 1 holds for all Jacobi polynomials $P(\alpha, \beta)$.*

The rate given in (33) provides a benchmark for any computational approach based on the tensor product expansion (29). The preeminent computational issue is the identification of these sets $\Lambda \subset (\mathbb{N}_0^\infty)_c$ that collect $|\Lambda|$ largest contributions of $\|u_\lambda\|_{H_0^1(D)}$, thus minimizing the expression on the left in (33). For this discussion, we define the non-increasing rearrangement $\bar{z} \in \ell^2(\mathbb{N})$ of the $H_0^1(D)$-norms of the Jacobi coefficients of the exact solution to the variational formulation (19) as the sequence

$$\bar{z}_k := \max_{|\Lambda| \leq k} \min_{\lambda \in \Lambda} \|u_\lambda\|_{H_0^1(D)}, \quad k \geq 1. \tag{34}$$

One of our goals is to numerically confirm the rate r given in (33).

2.5. Computation of mean and variance

The *expectation* operator $\mathbb{E}[\cdot]$ is defined as

$$\mathbb{E}[\cdot] := \int_\Gamma (\cdot)\, \rho(y)\, \mathrm{d}y. \tag{35}$$

For a function $u \in L^2_\rho(\Gamma; H_0^1(D))$ its *variance* $\mathbb{V}\mathrm{ar}[u]$ is defined by

$$\mathbb{V}\mathrm{ar}[u] := \mathbb{E}\left[u^2\right] - \mathbb{E}[u]^2. \tag{36}$$

The expansion (29) and orthonormality of the multivariate Jacobi polynomials in $L^2_\rho(\Gamma)$ imply that the expectation (35) and variance (36) of any $u \in L^2_\rho(\Gamma; H_0^1(D))$ can be written as

$$\mathbb{E}[u] = u_0 \quad \text{and} \quad \mathbb{V}\mathrm{ar}[u] = \sum_{\lambda \in (\mathbb{N}_0^\infty)_c \setminus \{0\}} u_\lambda^2, \tag{37}$$

where the subscript in u_0 refers to the all-zero multi-index.

Clearly, $\mathbb{E}[u] \in H_0^1(D)$. Further, the Sobolev embedding $H_0^1(D) \hookrightarrow L^{2q}(D)$ yields

$$\forall q \geq 1: \quad \exists C > 0: \quad \left\|u_\lambda^2\right\|_{L^q(D)} = \|u_\lambda\|^2_{L^{2q}(D)} \leq C\, \|u_\lambda\|^2_{H_0^1(D)}. \tag{38}$$

Thus, $(u_\lambda^2)_{\lambda \in (\mathbb{N}_0^\infty)_c}$ is a Cauchy sequence in $L^q(D)$, and $\mathbb{V}\mathrm{ar}[u] \in L^q(D)$ for any $q \geq 1$.

In the context of the p-finite element method, it is easy to compute the variance using the representation (37). Suppose $u_\lambda|_T = \sum_{i=0}^p c_i \varphi_i$ on a geometric element $T \subset \mathbb{R}^d$, with c_i being the coefficients and φ_k, $k \in \{0, 1, \cdots, 2p\}$, being linearly independent element shape functions. Assume there are coefficients $t_{ij,k} \in \mathbb{R}$ such that $\varphi_i \varphi_j = \sum_{k=0}^{2p} t_{ij,k} \varphi_k$ on T for all $0 \leq i \leq j \leq p$. Then

$$u_\lambda^2|_T = \sum_{i,j=0}^{p} c_i c_j \varphi_i \varphi_j = \sum_{k=0}^{2p} d_k \varphi_k \quad \text{with} \quad d_k = \sum_{i,j=0}^{p} c_i c_j t_{ij,k}. \tag{39}$$

3. Stochastic Reynolds Equation

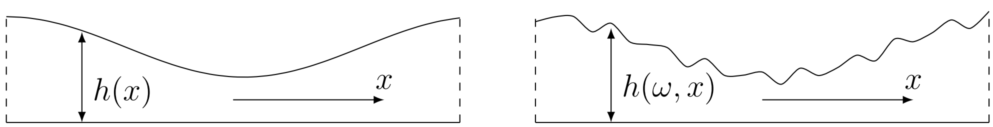

Figure 2: An illustration of the difference in the standard and stochastic film thicknesses. The depiction on the right represents one realization of the possible outcomes.

3.1. Journal Bearing Model

The geometric configuration is depicted in Figures 1 and 2. In the following two eccentricities are used throughout experiments: $\epsilon = 2/5$ and $\epsilon = 9/10$. The film thicknesses are shown in Figure 3 and the pressure profiles in the deterministic case in Figure 4.

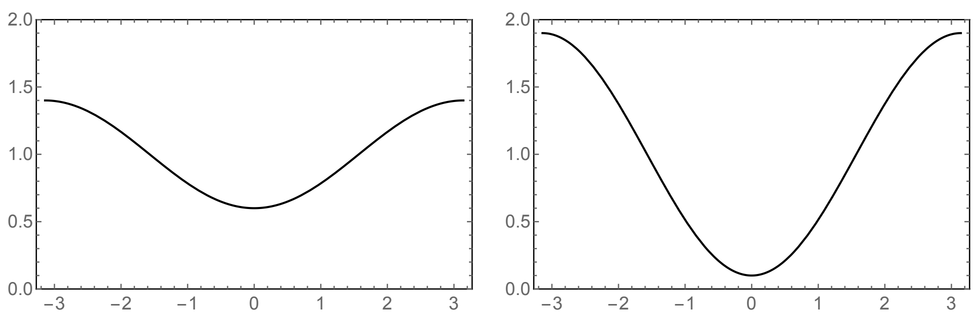

(a) $\epsilon = 2/5$. (b) $\epsilon = 9/10$.

Figure 3: Standard film thicknesses: $h(x) = 1 + \epsilon \cos(x + \pi)$.

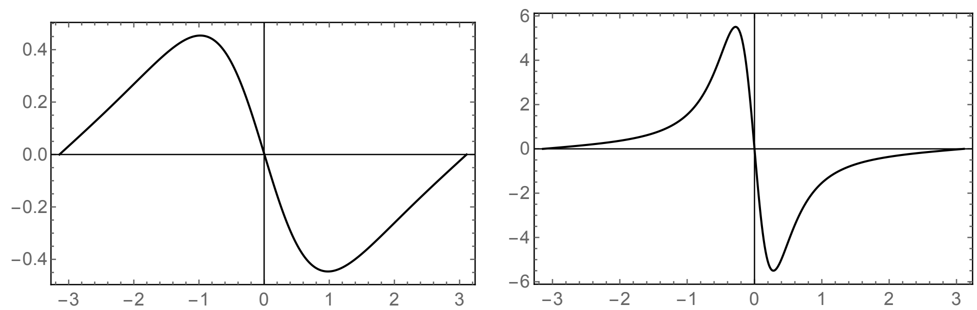

(a) $\epsilon = 2/5$. (b) $\epsilon = 9/10$.

Figure 4: Deterministic solution $p(x)$: $h(x) = 1 + \epsilon\cos(x+\pi)$.

3.2. Stochastic Model

In the stochastic model the input is the film thickness which is assumed to be random. It is introduced as a non-affine diffusion coefficient (cf. (16))

$$h(\omega, x) = 1 + \epsilon\cos(x+\pi) + \left(\sum_{m=1}^{M} \lambda_m \psi_m(x) Y_m(\omega)\right)^2, \tag{40}$$

where the deterministic functions $\psi_m(x)$ are the periodic covariance basis functions defined in Appendix A, and λ_m is a sequence decaying with some rate $\sigma > 1$, for instance, $\lambda_m = (1+m)^{-\sigma}$. This construction automatically guarantees the positivity of the variation in $h(x)$.

The spatial resolution of (40) is determined by the stochastic dimension M and the covariance length s (see Appendix A). Two sets of realizations are given in Figures 5 and 6. The former is a model of typical manufacturing imperfections and the latter describes wear and damage over the operation time of the bearing.

In the solutions of Figure 7 the effect of the perturbations is clearly visible. In contrast to the deterministic model (see Figure 4) the point of zero pressure can deviate from the origin. In the numerical experiments this will manifest itself as variance in the stochastic pressure field.

Formally the stochastic Reynolds equations becomes: Let (Ω, Σ, P) be a probability space. Find a random pressure field $p \in L^2_P(\Omega, H^1_0(D))$ such that

$$\frac{\partial}{\partial x}\left(\left[h(\omega,x)\right]^3 \frac{\partial p(\omega,x)}{\partial x}\right) = \frac{\partial h(\omega,x)}{\partial x}, \quad \text{in } D, \tag{41}$$

$$p(\omega, x) = 0, \qquad \text{on } \partial D. \tag{42}$$

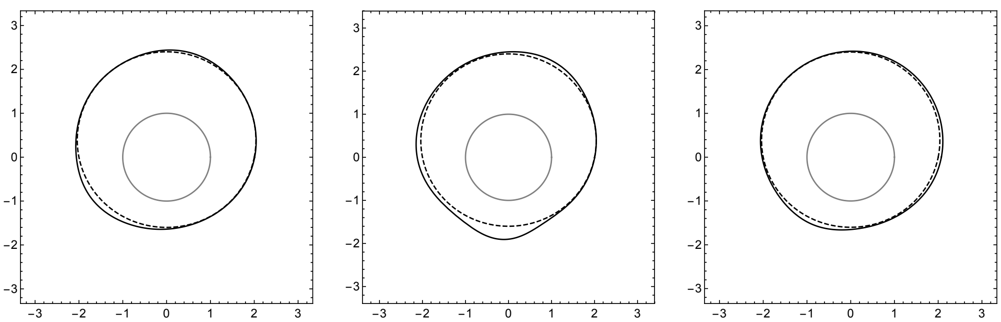

(a) (b) (c)

Figure 5: Realizations of $h(x)$: $\epsilon = 2/5$, $M = 10$, $\sigma = 1.05$, $s = 1/5$, $\alpha = \beta = 1/2$.

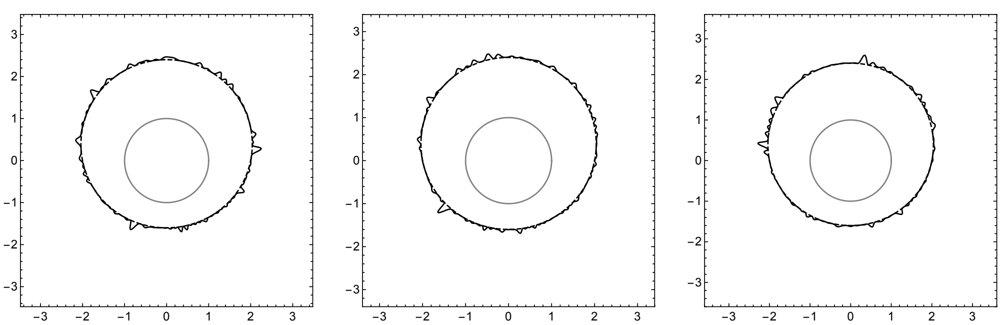

(a) (b) (c)

Figure 6: Realizations of $h(x)$: $\epsilon = 2/5$, $M = 100$, $C = 1/8$, $s = 1/100$, $\alpha = \beta = 1/2$.

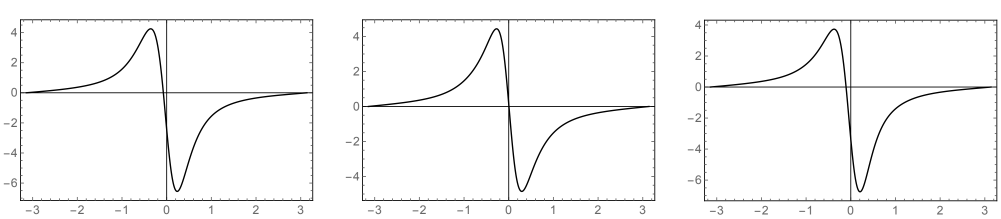

(a) (b) (c)

Figure 7: Realizations of $p(x)$: $\epsilon = 9/10$, $M = 10$, $\sigma = 1.05$, $s = 1/5$, $\alpha = \beta = 1/2$.

Expanding the term $\left[h(\omega,x)\right]^3$ we end up with a sum with four terms. In this paper this sum is approximated with a *reduced model*

$$\left[h(\omega,x)\right]^3 \approx (1+\epsilon\cos(x+\pi))^3 + \left(\sum_{m=1}^{M}\lambda_m\psi_m(x)Y_m(\omega)\right)^6 . \tag{43}$$

This reduction is motivated by computational concerns only. The remaining two terms are representative of those appearing in stochastic Galerkin computations. Yet, from the point of view of implementation complexity, the reduced model has the highest power of the series. The *curse of dimension* enters at this point in the number of terms in the expanded polynomial.

4. Numerical Experiments

The numerical experiments have been divided into two parts. In all experiments the stochastic dimension is fixed, $M = 10$, resulting in 5005 terms in the expanded polynomial, and the set of multi-indices Λ is chosen using the total degree strategy (see Definition 6) where the degree K is even. In fact, as a consequence of (43), only multi-indices of even degree are included in Λ. In the first part the effects and interdependence of the degree K, rate σ, and eccentricity ϵ are studied. One of the cases is also validated using a Monte Carlo approach. In the second part some individual parameters such as the deterministic polynomial order p, or the choice of stochastic parameter distribution are examined.

4.1. Experimental Setup

In the basic setup the mesh is fixed with the mesh parameter $2\pi/100$ and $p = 4$ (uniform). The covariance length is $s = 1/5$ and the periodic covariance functions are computed as in the Appendix A. The stochastic parameters are assumed to be distributed as $\sim 2\sqrt{2}\,\mathrm{Beta}(\alpha+1,\beta+1)-1 \in [-1,1]$, with $\alpha = \beta = -1/2$ and thus, the chaos polynomials are the normalized Jacobi polynomials $P(-1/2,-1/2)$. The sequence λ_m in (40) is $\lambda_m = (1+m)^{-\sigma}$. In all cases the linear systems of equations are solved using the preconditioned conjugate gradient algorithm outlined in Appendix B. The right-hand-side of (41) can either be $\partial\mathbb{E}[h(\omega,x)]/\partial x$ (deterministic) or $\partial h(\omega,x)/\partial x$ (stochastic). Notice, that in the deterministic case only a first-order approximation of the mean is used. All computations are carried out with Mathematica 11 [29].

Case	K	ϵ	σ	$\|\Lambda\|$	$\|\mathbb{E}(u)\|_{L^2}$	$\|\mathbb{E}(u)\|_{H^1}$	$\|\mathrm{Var}(u)\|_{L^2}$
1	2	2/5	2	56	0.753854	0.872351	2.30321×10^{-13}
2	6	2/5	2	5776	0.753854	0.872351	3.07196×10^{-13}
3	2	2/5	1.05	56	0.753761	0.872210	3.56805×10^{-8}
4	6	2/5	1.05	5776	0.753761	0.872210	5.4521×10^{-8}
5	2	9/10	2	56	5.411410	18.54060	7.44175×10^{-7}
6	6	9/10	2	5776	5.411410	18.54060	9.72236×10^{-7}
7	2	9/10	1.05	56	5.340150	18.08820	0.0511959
8	6	9/10	1.05	5776	5.342960	18.10700	0.0519018

(a) Deterministic RHS.

Case	K	ϵ	σ	$\|\Lambda\|$	$\|\mathbb{E}(u)\|_{L^2}$	$\|\mathbb{E}(u)\|_{H^1}$	$\|\mathrm{Var}(u)\|_{L^2}$
9	2	2/5	2	56	0.753854	0.872351	0.000177478
10	2	9/10	1.05	56	5.311790	17.93820	6.182000

(b) Stochastic RHS.

Table 1: Summary of basic numerical experiments: $M = 10$, $p = 4$, $s = 1/5$, mesh parameter is $2\pi/100$.

4.2. Cases

The different cases are summarized in Table 1. In order to avoid confusion with the polynomial degree p, the computed solution is referred to as u. Notice that in Figure 7 the three realizations differ in the vicinity of the origin. Therefore it is to be expected that the maximal variance is centered around the origin. This feature is illustrated in the variance plots for deterministic and stochastic RHS's in Figures 8 and 9, respectively.

Let us next consider the effects of different parameters. For fixed (ϵ, σ)-pairs, the increase in the total degree K leads to higher variance. Similarly, larger eccentricity ϵ and lower rate σ have the same effect. It is also notable that the support of the variance is larger for a lower value of ϵ.

Including uncertainty also in the RHS increases the variance significantly, in fact over two orders of magnitude. This is again intuitively clear since the derivatives of the film thickness include stronger oscillations. Considering the maximal variance in Figure 9b one can interpret the corresponding maximal standard deviation as the shift in the location of the maximal pressure drop away from the origin. This has been illustrated in Figure 10 where both the expected pressure field and one standard deviation are shown together.

In Figure 11 the convergence of Jacobi coefficients is illustrated with

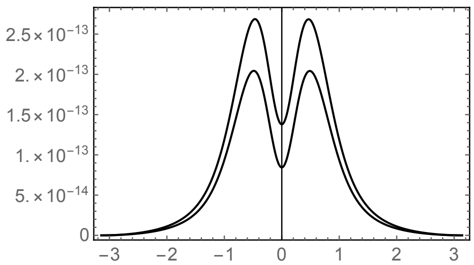

(a) Cases 1 and 2: $\epsilon = 2/5$, $\sigma = 2$.

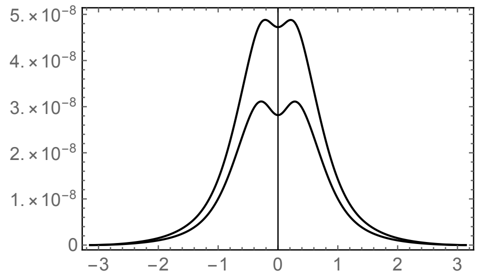

(b) Cases 3 and 4: $\epsilon = 2/5$, $\sigma = 1.05$.

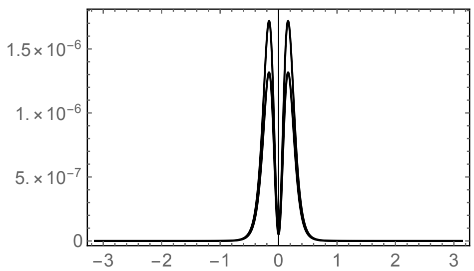

(c) Cases 5 and 6: $\epsilon = 9/10$, $\sigma = 2$.

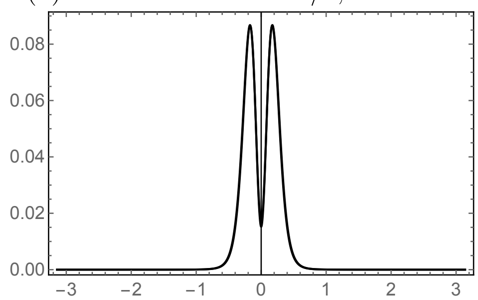

(d) Cases 7 and 8: $\epsilon = 9/10$, $\sigma = 1.05$.

Figure 8: Variance: Deterministic RHS; In all cases larger K leads to higher variance.

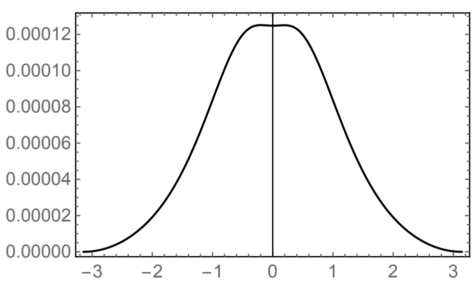

(a) Case 9: $\epsilon = 2/5$, $\sigma = 2$.

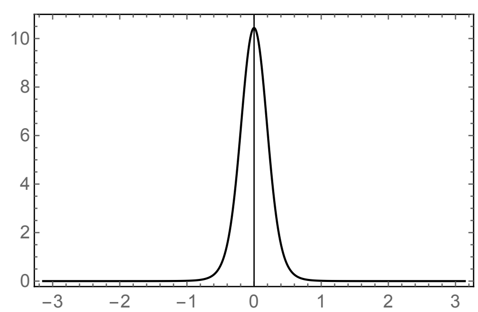

(b) Case 10: $\epsilon = 9/10$, $\sigma = 1.05$.

Figure 9: Variance: Stochastic RHS.

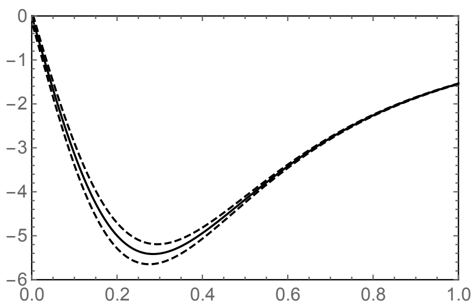

(a) Case 8: Detail.

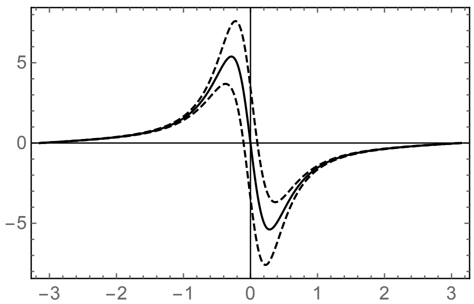

(b) Case 10.

Figure 10: Stochastic pressure fields: Expectation and one standard deviation (dashed).

asymptotic $\bar{z}_k$ convergence plots. In all subfigures two overlapping graphs representing degrees $K = 2$ and $K = 6$ give an indication of the relative success of the multi-index selection scheme. Since the two sets of multi-indices are hierarchic, one can find the approximate positions of the elements of the smaller set within the larger one by comparing Jacobi coefficients. For instance, in Figure 11c the "branching point" occurs already after the first five multi-indices, whereas in Figure 11d in a more challenging case (smaller σ) branching occurs later. This means that for $\epsilon = 9/10$, $\sigma = 2$ it is likely that a more efficient scheme for selecting the optimal Λ could be devised.

The preconditioner used in the conjugate gradient algorithm performed remarkably well. The cases with $K = 6$ had 7,260,432 degrees of freedom, and the number of steps varied from 3 to 13 iterations steps in Case 8, with tolerance 10^{-6}. On Apple Mac Pro 2009 Edition 2.26 GHz one step took 12 minutes without parallelization.

4.3. Monte Carlo Validation

The Case 8 has also been solved using standard Monte Carlo (MC) approach using exactly the same experimental setup per realization. In Figure 12 the MC L^2-convergence graphs for both the expected solution and variance are shown. In both cases the graphs convergence as $O(N^{-1/2})$, when the reference values are the respective Galerkin solutions. This result strengthens our confidence that the Galerkin results are correct.

4.4. Special Cases

Unless otherwise specified, in this section the baseline experiment is the Case 8 above.

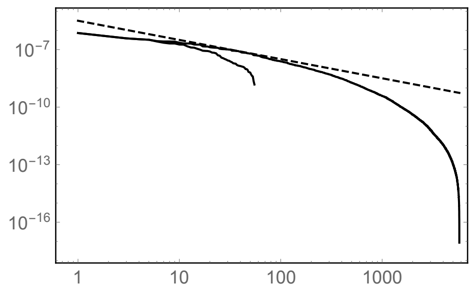

(a) Cases 1 and 2: $\epsilon = 2/5$, $\sigma = 2$.

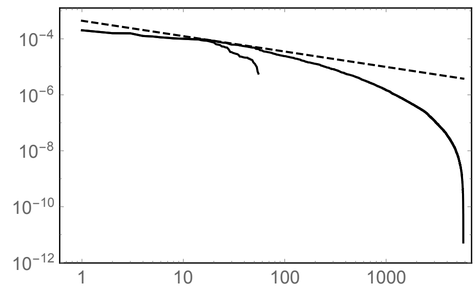

(b) Cases 3 and 4: $\epsilon = 2/5$, $\sigma = 1.05$.

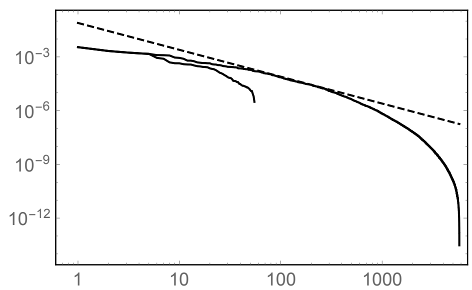

(c) Cases 5 and 6: $\epsilon = 9/10$, $\sigma = 2$.

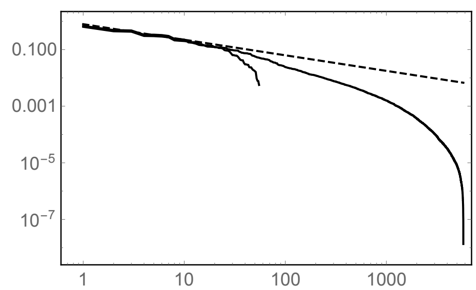

(d) Cases 7 and 8: $\epsilon = 9/10$, $\sigma = 1.05$.

Figure 11: Convergence of Jacobi coefficients: $\bar{z}_k$-plots; Two overlapping graphs representing degrees $K = 2$ and $K = 6$; The dashed line is the best upper bound with the rate $\sigma - 1/2$.

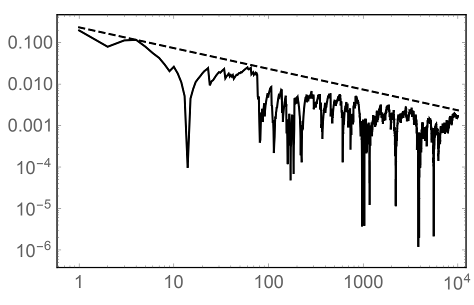

(a) Expectation.

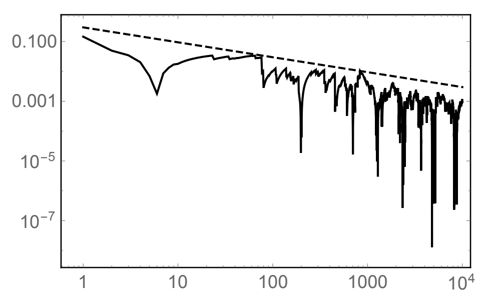

(b) Variance.

Figure 12: Monte Carlo: Configuration of Case 8; Convergence in L^2-norm over 10000 trials; The dashed line is the best upper bound with the rate $r = 1/2$, error $\leq C\,N^{-r}$.

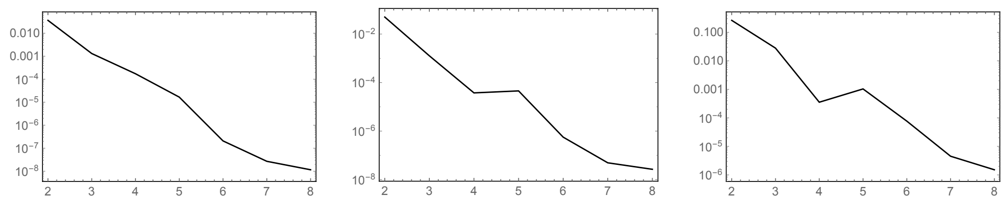

(a) $\|\mathbb{E}(u)\|_{L^2}$ (b) $|\mathbb{E}(u)|_{H^1}$ (c) $\|\mathrm{Var}(u)\|_{L^2}$

Figure 13: p-Version: Convergence of the p-version; Norm as a function of p; log-plot.

4.4.1. p-Version

In the experiments above, the discretization of the deterministic part is kept fixed. In this experiment the mesh is refined around the origin with the ratio of 1/100. The polynomial order is uniform over the mesh, $p \in \{2, \cdots, 8\}$. The convergence graphs in different norms are given in Figure 13. With the reference results obtained from an overkill solution, the convergence rates are exponential almost over the whole range of p. In the H^1-seminorm there is a clear odd/even-effect in the convergence graph with corresponding oscillations in the convergence of the variance. This oscillation is an indication of the least squares -type convergence of the higher statistical moments.

Although the theoretical foundation of the preconditioner is based on h-type FEM analysis, our results suggest that it is also *p-robust*. The iteration count over the range of experiments, $p \in \{2, \cdots, 8\}$, was constant.

4.4.2. Short Covariance Length

If the covariance length is changed from $s = 1/5$ to $s = 1/20$, the covariance function will have a smaller maximal amplitude. Hence, in the numerical experiment the computed variance should be smaller. This is indeed the case, with $\|\mathrm{Var}(u)\|_{L^2} = 5.6964 \times 10^{-5}$.

4.4.3. Nonsymmetric Beta Distribution

Conjecture 2 suggests that the choice of α and β should not affect the $\bar{z}_k$ convergence rate. The results given in Table 2 support this. The experiments have been repeated with three nonsymmetric (α, β)-pairs. The quantities of interest are not constant, yet the $\bar{z}_k$-convergence rates are the same, at least with the relatively modest stochastic dimension $M = 10$.

Case	α	β	$\|\mathbb{E}(u)\|_{L^2}$	$\|\mathbb{E}(u)\|_{H^1}$	$\|\mathrm{Var}(u)\|_{L^2}$
A	1	2	5.40449	18.4949	8.98886×10^{-4}
B	-2/3	-1/3	5.40949	18.5278	5.57219×10^{-5}
C	-4/5	-1/6	5.23418	17.4062	0.0517587
D	-1/4	-3/4	5.27461	17.6657	0.0563149

(a) Quantities of interest.

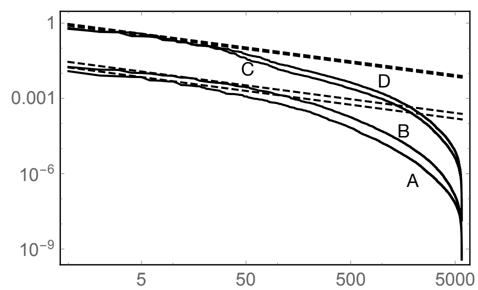

(b) Asymptotic $\bar{z}_k$-convergence graphs. The graphs of C and D are essentially overlapping, and those of A and B share the same characteristics.

Table 2: Convergence of Jacobi coefficients: Configuration of Case 8.

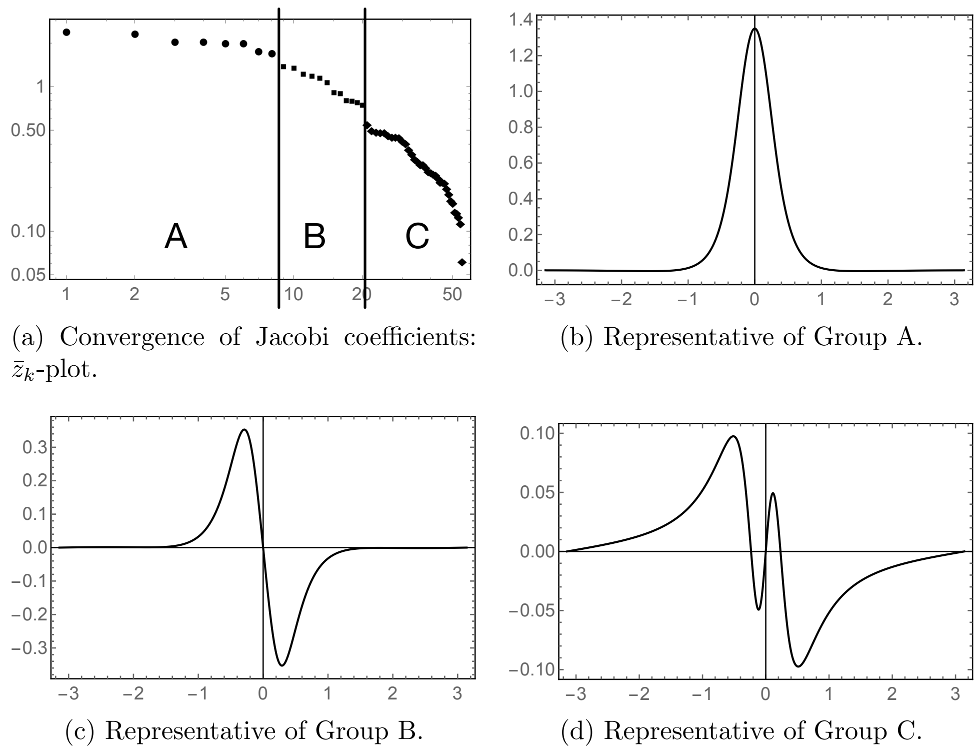

(a) Convergence of Jacobi coefficients: $\bar{z}_k$-plot.

(b) Representative of Group A.

(c) Representative of Group B.

(d) Representative of Group C.

Figure 14: Case 10: Characteristics of Jacobi coefficients: The Jacobi coefficients can be illustrated as FEM-solutions. Since the coefficients in the group A have higher $\bar{z}_k$ values it is clear why the variance graph of Figure 9b has a strong resemblance. The higher oscillations present in coefficients in the group C have smaller $\bar{z}_k$ values.

4.4.4. Multi-Indices: $\bar{z}_k$

Finally, let us examine in detail the connection between the multi-indices and their respective $\bar{z}_k$ values. In Figure 14a the $\bar{z}_k$-plot of the Case 10 is shown. Three groups of multi-indices can be identified, and their representative examples are shown in other subfigures of Figure 14. The variance graph of Figure 9b is a linear combination of the Jacobi coefficients modulo the first one, the expected value. Simply by comparing the shapes of the Jacobi coefficients with the variance it is clear that in this case the higher oscillations must have smaller $\bar{z}_k$ values.

5. Conclusions and Discussion

In this paper the approximation of the Reynolds equation with a stochastic film thickness has been discussed. The necessary computational framework has been outlined and its performance has been demonstrated over a series of numerical experiments. The framework provides practicing engineers and modelers additional flexibility for incorporating random variables with a wide variety of distributions within the same stochastic Galerkin method.

The numerical results also indicate further theoretical research directions. The preconditioned conjugate gradient method performs well and could be shown to be p-robust. Within the range of practical polynomial orders our results support this. Similarly, it remains open theoretically whether the results on the asymptotics of the Legendre polynomials can be generalized for all Jacobi polynomials.

The results suggest that the stochastic Galerkin method is capable of supporting design when the manufacturing imperfections (larger scale variations) are the main sources of uncertainty. It remains a challenge to include wear and damage (smaller scale variations) to practical numerical simulations. In order to introduce the different characteristic length scales one has to either increase the stochastic dimension M or achieve a similar effect with an additional multiplicative factor. In either case the curse of dimensionality will increase the computational requirements significantly. Also, in more realistic scenarios with 2D surfaces, say, the same constraints are met even earlier.

Appendix A. On the Construction of Periodic covariance

Appendix A.1. Fourier transform of periodic function

Assume $f(x)$ is a periodic function with period $2L$. Any periodic function can be expressed as the sum of a series of sines and cosines:

$$f(x) = \frac{a_0}{2} + \sum_{n=1}^{\infty} a_n \cos\left(\frac{n\pi x}{L}\right) + b_n \sin\left(\frac{n\pi x}{L}\right),$$

where

$$a_n = \frac{1}{L}\int_{-L}^{L} f(x)\cos\left(\frac{n\pi x}{L}\right) \mathrm{d}x, \quad n = 0, 1, 2, \ldots$$

and

$$b_n = \frac{1}{L}\int_{-L}^{L} f(x)\sin\left(\frac{n\pi x}{L}\right)\mathrm{d}x, \quad n = 1, 2, \ldots$$

If the function $f(x)$ is even, $b_n = 0$. We recall the following identity that will be useful later on:

$$\cos(x_2 - x_1) = \cos(x_1)\cos(x_2) + \sin(x_1)\sin(x_2).$$

1 *Appendix A.2. KL-expansion*

KL-expansion is typically written as

$$a(\omega, x) = \Psi_0(x) + \sum_{k=1}^{\infty} \Psi_k(x) Y_k(\omega),$$

where $\{\Psi_k\}_{k=1}^{\infty}$ are some suitable functions, $\mathbb{E}[Y_k] = 0$, and $\mathbb{E}[Y_k Y_l] = \delta_{kl}$. The idea is to choose $\{\Psi_k\}_{k=1}^{\infty}$ so that $a(\omega, x)$ has some desired structure. The expectation of $a(\omega, x)$ is given by

$$\mathbb{E}[a(\omega, x)] = \Psi_0(x)$$

and the covariance of $a(\omega, x)$ equals

$$\begin{aligned} c_a(x_1, x_2) &= \mathbb{E}\left[(a(\omega, x_1) - \mathbb{E}[a(\omega, x_1)])(a(\omega, x_2) - \mathbb{E}[a(\omega, x_2)])\right] \\ &= \mathbb{E}\left[\left(\sum_{k=1}^{\infty} \Psi_k(x_1) Y_k(\omega)\right)\left(\sum_{k=1}^{\infty} \Psi_k(x_2) Y_k(\omega)\right)\right] \\ &= \sum_{k=1}^{\infty} \Psi_k(x_1)\Psi_k(x_2). \end{aligned}$$

2 *Appendix A.3. Periodic covariance*

Let

$$c(\lambda, s) = \exp\left(-\frac{\lambda^2}{2s^2}\right)$$

be the covariance that we use to construct a $2L$-periodic covariance denoted by $c_a(\lambda, s, L)$. By defining

$$c_a(\lambda, s, L) = \sum_{k=-\infty}^{\infty} c(\lambda + 2Lk, s),$$

the covariance c_a is periodic with period $2L$ and even. Now the Fourier coefficients $a_n(s,L)$ are

$$\begin{aligned} a_n(s,L) &= \frac{1}{L}\int_{-L}^{L} c_a(\lambda,s,L)\cos\left(\frac{n\pi\lambda}{L}\right)\mathrm{d}\lambda \\ &= \frac{1}{L}\sum_{k=-\infty}^{\infty}\int_{-L}^{L}\exp\left(-\frac{(\lambda+2Lk)^2}{2s^2}\right)\cos\left(\frac{n\pi\lambda}{L}\right)\mathrm{d}\lambda \\ &= \frac{1}{L}\sum_{k=-\infty}^{\infty}\int_{(2k-1)L}^{(2k+1)L}\exp\left(-\frac{y^2}{2s^2}\right)\cos\left(\frac{n\pi y}{L}-\frac{2Lkn\pi}{L}\right)\mathrm{d}y \\ &= \frac{1}{L}\sum_{k=-\infty}^{\infty}\int_{(2k-1)L}^{(2k+1)L}\exp\left(-\frac{y^2}{2s^2}\right)\cos\left(\frac{n\pi y}{L}\right)\mathrm{d}y \\ &= \frac{1}{L}\int_{\mathbb{R}}\exp\left(-\frac{y^2}{2s^2}\right)\cos\left(\frac{n\pi y}{L}\right)\mathrm{d}y \\ &= \frac{\sqrt{2\pi}s}{L}\exp\left(-\frac{n^2s^2\pi^2}{2L^2}\right) \end{aligned}$$

and we have

$$c_a(\lambda,s,L) = \frac{a_0(s,L)}{2} + \sum_{n=1}^{\infty} a_n(s,L)\cos\left(\frac{n\pi\lambda}{L}\right).$$

By defining $c_a(x_1,x_2,s,L) = c_a(x_2-x_1,s,L)$, we have

$$\begin{aligned} c_a(x_1,x_2,s,L) = \frac{a_0(s,L)}{2} &+ \sum_{n=1}^{\infty} a_n(s,L)\cos\left(\frac{n\pi}{L}x_1\right)\cos\left(\frac{n\pi}{L}x_2\right) \\ &+ \sum_{n=1}^{\infty} a_n(s,L)\sin\left(\frac{n\pi}{L}x_1\right)\sin\left(\frac{n\pi}{L}x_2\right). \end{aligned}$$

By defining

$$\Psi_1(x,s,L) = \sqrt{\frac{a_0(s,L)}{2}}, \tag{A.1}$$

$$\Psi_{2j}(x,s,L) = \sqrt{a_j(s,L)}\cos\left(\frac{j\pi}{L}x\right), \text{ and} \tag{A.2}$$

$$\Psi_{2j+1}(x,s,L) = \sqrt{a_j(s,L)}\sin\left(\frac{j\pi}{L}x\right), \tag{A.3}$$

where $j \geq 1$, the KL-expansion

$$a(\omega, x) = \Psi_0(x) + \sum_{k=1}^{\infty} \Psi_k(x) Y_k(\omega),$$

has the covariance $c_a(x_1, x_2, s, L)$. Notice that we can choose Ψ_0 as we like.

Appendix B. Conjugate Gradients

The linear systems of the type (25) lend themselves naturally to iterative methods. There are two advantages: the action of the operator (matrix-vector multiply) can be written in a matrix-free fashion and, more importantly, block-diagonal preconditioner of the form $I \otimes A_0^{-1}$ is highly effective [30].

In practice, the implementation of the preconditioned conjugate gradients is straightforward. Although the linear systems (25) are inherently sparse, by judiciously folding and unfolding the temporary vectors and matrices, respectively, many computations can in fact be computed using full matrix-matrix routines. One such implementation is outlined in Figure B.15.

References

[1] D. Xiu, Numerical Methods for Stochastic Computations: A Spectral Method Approach, Princeton University Press, Princeton, N.J., 2010.

[2] M. Bieri, Ch. Schwab, Sparse high order FEM for elliptic sPDEs, Comput. Methods Appl. Mech. Engrg. 198 (2009) 1149–1170.

[3] P. G. Ciarlet, Mathematical Elasticity, Volume II: Theory of Plates, North-Holland, 1997.

[4] S. Timoshenko, J. Goodier, Theory of Elasticity, McGraw, New York, 1970.

[5] A. Z. Szeri, Fluid Film Lubrication, Second Edition, Cambridge University Press, 2011.

[6] P. Martin, On Webster's horn equation and some generalizations, The Journal of the Acoustical Society of America 116 (2004) 1381–1388.

Preconditioner $M(\cdot)$

Require: Matrix A_0, vector b.

```
Solve A_0 X = Folded column-wise b
return Unfolded X
```

Matrix-vector multiply $A(\cdot)$

Require: Matrices A_i, G_i, $i = 1, \ldots$, vector x. G_0 is assumed to be an identity matrix.

```
U := Folded column-wise x
V := A_0 U + \sum_i G_i U^T A_i^T
return Unfolded V
```

Algorithm

Require: Matrix-vector multiply: $A(\cdot)$; Preconditioner: $M(\cdot)$.

```
Compute r_0 := b − A(x_0), z_0 := M(r_0), p_0 := z_0,
for j = 0, 1, ..., until convergence do
    α_j := (r_j, r_j)/(A(p_j), p_j)
    x_{j+1} := x_j + α_j p_j
    r_{j+1} := r_j − α_j A(p_j)
    z_{j+1} := M(r_{j+1})
    β_j := (z_{j+1}, r_{j+1})/(z_j, r_j)
    p_{j+1} := z_{j+1} + β_j p_j
end for
return x
```

Figure B.15: The preconditioned conjugate gradient algorithm.

[7] H. Hakula, M. Leinonen, On efficient construction of stochastic moment matrices, arXiv preprint arXiv:1502.07562 (2015).

[8] O. Reynolds, On the theory of lubrication and its application to Mr Tower's experiments, Philosophical Transactions of the Royal Society of London 177 (1886).

[9] B. J. Hamrock, S. R. Schmid, B. O. Jacobson, Fundamentals of Fluid Film Lubrication, Second Edition, Marcel Dekker, Inc., 2004.

[10] S. Tzeng, E. Saibel, Surface roughness effect on slider bearing lubrication, Asle Transactions 10 (1967) 334–348.

[11] H. Christensen, Stochastic models for hydrodynamic lubrication of rough surfaces, Proceedings of the Institution of Mechanical Engineers 184 (1969).

[12] S. K. Rhow, H. G. Elrod, The effects on bearing load-carrying capacity of two-sided striated roughness, Journal of Lubrication Technology 96 (1974) 554–558.

[13] N. Patir, H. Cheng, An average flow model for determining effects of three-dimensional roughness on partial hydrodynamic lubrication, Journal of lubrication Technology 100 (1978) 12–17.

[14] N. Patir, H. Cheng, Application of average flow model to lubrication between rough sliding surfaces, Journal of Lubrication Technology 101 (1979) 220–229.

[15] S. Wu, J. Oden, Studies in convergence of stochastic models in rough-surface hydrodynamic lubrication theory, International journal of engineering science 23 (1985) 235–240.

[16] G. Bayada, I. Ciuperca, M. Jai, Homogenized elliptic equations and variational inequalities with oscillating parameters. application to the study of thin flow behavior with rough surfaces, Nonlinear analysis: real world applications 7 (2006) 950–966.

[17] A. Almqvist, J. Fabricius, A. Spencer, P. Wall, Similarities and differences between the flow factor method by Patir and Cheng and homogenization, Journal of tribology 133 (2011) 031702.

[18] G. Kabacaoğlu, İ. Temizer, Homogenization of soft interfaces in time-dependent hydrodynamic lubrication, Computational Mechanics 56 (2015) 421–441.

[19] R. Turaga, A. Sekhar, B. Majumdar, Stability analysis of a rigid rotor supported on hydrodynamic journal bearings with rough surfaces using the stochastic finite element method, Proceedings of the Institution of Mechanical Engineers, Part J: Journal of Engineering Tribology 212 (1998) 121–130.

[20] R. Turaga, A. Sekhar, B. Majumdar, Stochastic FEM model of one-dimensional hydrodynamic bearings with rough surfaces, Wear 197 (1996) 221–227.

[21] R. Turaga, Stochastic FEM analysis of finite hydrodynamic bearings with rough surfaces, Tribology transactions 40 (1997) 605–612.

[22] D. Xiu, J. Shen, An efficient spectral method for acoustic scattering from rough surfaces, Commun. Comput. Phys 1 (2007) 54–72.

[23] C. Bierig, A. Chernov, Convergence analysis of multilevel monte carlo variance estimators and application for random obstacle problems, Numerische Mathematik 130 (2015) 579–613.

[24] N. Hyvönen, L. Mustonen, Thermal tomography with unknown boundary, arXiv preprint arXiv:1611.06862 (2016).

[25] R. J. Adler, J. E. Taylor, Random Fields and Geometry, volume 115 of *Springer monographs in mathematics*, Springer, New York, 2007.

[26] A. Chkifa, A. Cohen, Ch. Schwab, Breaking the curse of dimensionality in sparse polynomial approximation of parametric PDEs, J. Math. Pures Appl. 103 (2015) 400–428.

[27] Ch. Schwab, C. J. Gittelson, Sparse tensor discretizations of high-dimensional parametric and stochastic PDEs, Acta Numer. 20 (2011) 291–467.

[28] A. Cohen, R. DeVore, Ch. Schwab, Analytic regularity and polynomial approximation of parametric and stochastic elliptic PDE's, Anal. Appl. 9 (2011) 11–47.

[29] Inc. Wolfram Research, Mathematica, version 11.0, 2016.

[30] C. E. Powell, H. C. Elman, Block-diagonal preconditioning for spectral stochastic finite-element systems, IMA Journal of Numerical Analysis 29 (2008) 350–375.